Journal of MATERIALS RESEARCH

Invited Feature Paper
DOI: 10.1557/jmr.2019.232

Ultra-rapid microwave sintering employing thermal instability and resonant absorption

Kirill I. Rybakov[1,a], Sergei V. Egorov[1], Anatoly G. Eremeev[1], Vladislav V. Kholoptsev[1], Ivan V. Plotnikov[1], Andrei A. Sorokin[1]

[1]*Institute of Applied Physics, Russian Academy of Sciences, Nizhny Novgorod 603950, Russia*
[a)]Address all correspondence to this author. e-mail: rybakov@appl.sci-nnov.ru
This paper has been selected as an Invited Feature Paper.
Received: 29 April 2019; accepted: 25 June 2019

Ultra-rapid microwave sintering of ceramics has been recently demonstrated by the authors. In the experiments with oxide ceramic samples carried out in a 24 GHz gyrotron system for microwave processing of materials, full density was achieved in the sintering processes with a duration of the high-temperature stage of one to several minutes and zero hold at the maximum temperature. The implementation of the ultra-rapid microwave sintering processes was made possible due to fast and efficient control over the temperature of the materials and the supplied microwave power. The absorbed microwave power density was typically in the range of 10–100 W/cm^3, which is within the same order of magnitude as the power of Joule heat in the DC electric field–assisted flash sintering processes. At this power level, a thermal instability is triggered by the volumetric heating, which results in a drastic enhancement of mass transport. In addition, possibility of ultra-rapid microwave sintering of powder metals has been demonstrated within a model accounting for the effective electromagnetic properties and resonant absorption effects.

Introduction

Microwave sintering of materials has been under active study for more than thirty years, with first experiments undertaken back in the 1960s [1, 2, 3, 4, 5]. Since the early studies, it has been claimed that microwave heating has a potential of enhancing the rate of the sintering process [6]. Among the proposed reasons for that were the volumetric nature of microwave absorption and the non-thermal effects associated with the interaction of the electromagnetic field with solids [7, 8, 9, 10, 11].

The power deposited volumetrically within the sample is spent on increasing its internal energy and on compensating the heat losses from the sample. The heating rate generally increases with the increase in the deposited power density. There have been many experimental studies in which relatively high heating rates, on the order of 100 °C/min, were achieved using microwave heating (e.g., [12, 13, 14]). However, in many ceramic materials, an increase in the volumetrically deposited power above a certain threshold usually causes development of thermal instability. In most cases, it is associated with the positive feedback between the power and the temperature occurring due to the rising dependence of the material's effective electric conductivity (or microwave absorptivity) on temperature.

Since the first studies of microwave processing of ceramics, the thermal instability has been known as an undesired effect [15]. Under a fixed power of microwave irradiation, the thermal instability, also known as the temperature runaway, manifests itself as a very rapid increase in the heating rate. Within a very short time, the temperature reaches prohibitively high values leading to melting and/or destruction of the sample. In practical terms, in addition to the shape of the effective conductivity versus temperature curve, the development of thermal instability during microwave sintering depends on many factors determining the release and loss of heat, such as the thermal conductivity of the sample [16], the real part of the material's dielectric permittivity [17], the configuration and properties of the thermal insulation arrangement used in the experiments, and reactions and phase transformations accompanied by release or absorption of energy.

https://doi.org/10.1557/jmr.2019.232 Published online by Cambridge University Press

© Materials Research Society 2019

There have been a considerable number of studies of the conditions and regimes of the development of thermal instabilities under microwave heating. The aim of most studies was to isolate the domains of parameters in which the instability does not develop [18] or to suggest means of efficient control and suppression of the instability [19, 20]. Depending on the relationship between the rate of the volumetric power dissipation in the material and the rate of power removal via different channels of heat losses, the instability can develop within the sample globally or locally. The global development of the instability, i.e., a rapid growth of temperature within the entire sample, can be suppressed by introducing a negative feedback loop regulating the microwave power based on the signal from a sensor that measures the surface temperature of the sample. However, when the effective conductivity of a material exhibits a sharper growth with the increasing temperature, the thermal instability can develop in a localized internal region of the sample (the so-called hot spot). In this case, the instability cannot be detected and suppressed by the control systems based on surface temperature measurements [21].

In parallel with the development of microwave sintering, other sintering methods employing application of electromagnetic field, generally termed field-assisted sintering techniques, have been under development over the last decades [22, 23, 24, 25]. More recently, the method of flash sintering, resulting in ultra-rapid densification of powder materials, has received considerable research attention [26, 27, 28]. In the most common implementations of this method, a DC or low-frequency AC electric voltage is applied (with the help of electrodes) to a powder compact undergoing heating in a conventional furnace. After a certain incubation period (which is needed to reach the necessary temperature and electric current density), a thermal instability develops in the material due to volumetric Joule heating. The electric power supply is then switched into the current control mode, and the sample is held at high temperature for a certain time. The densification predominantly occurs during the stage of the thermal instability development. In some cases, full densification is achieved on the time scale on the order of several seconds. Therefore, in flash sintering the thermal instability is used purposely as a method to implement ultra-rapid heating and sintering [29].

In recent years, ultra-rapid sintering processes have been implemented under microwave heating, making use of the precisely controlled thermal instability to achieve high rates of both heating and densification [30, 31, 32, 33, 34, 35, 36, 37]. This paper briefly reviews the results achieved in this field and provides additional experimental evidence. "Ultra-rapid microwave sintering of ceramics using thermal instability" section describes ultra-rapid processes in which the thermal instability is allowed to develop freely until the ceramic material reaches a certain permissible maximum temperature. In the processes described in "Ultra-rapid microwave sintering at constant heating rates with compensated thermal instability" section, the development of thermal instability is mediated by the automatic control over the microwave power, which makes it possible to sustain high rates of heating and densification. "Ultra-rapid microwave sintering of metal powders using resonant absorption" section discusses the possibility of implementing similar ultra-rapid microwave heating processes in the samples compacted from metal powders via purposeful use of resonant microwave absorption.

Ultra-rapid microwave sintering of ceramics using thermal instability

A straightforward way to employ thermal instability for the implementation of ultra-rapid microwave sintering is to expose the sample to high-power microwave radiation while monitoring the temperature of the sample to turn the microwave power off when a maximum permissible temperature is reached. The value of the permissible temperature is selected based on preliminary experiments to exclude melting and/or destruction of the sample due to overheating. Perhaps, one of the first observations of accidental ultra-rapid microwave sintering was made in 2007 in a study of the microwave sintering of Nd:Y_2O_3 laser ceramics undertaken by the authors jointly with the team of the Institute of Electrophysics (Ekaterinburg, Russia). The sintering process normally involved slow heating at a rate of 5 °C/min to 1750 °C and a hold at this temperature for 10 h, and it resulted in obtaining transparent ceramic samples with a very low residual porosity. However, in one of the experiments, a temperature runaway occurred unexpectedly, and the process was terminated automatically by the control system on reaching a temperature of 1600 °C. The total time spent by this sample at high temperature (at which densification could proceed) was on the order of 15 s. Surprisingly, the sample obtained in this experiment was transparent (although its optical transmission properties were worse than those of the samples that were sintered for 10 h), which means that it had quite little porosity remaining. The density of this sample—which in fact was obtained by ultra-rapid microwave sintering with an achieved reduction in the sintering time by a factor of more than 2000—exceeded 99.5% of the theoretical value [36].

The described observation has demonstrated that sintering of ceramics to virtually full density can in principle be achieved within a very short time during the thermal instability development, without the need in additional high-temperature hold. A series of experiments on the ultra-rapid microwave

https://doi.org/10.1557/jmr.2019.232 Published online by Cambridge University Press

© Materials Research Society 2019

sintering making purposeful use of the thermal instability was undertaken with $(Yb_{0.05}Y_{0.85}La_{0.1})_2O_3$ laser ceramics [30, 31]. After the samples were brought to a temperature of 800 °C and held at this temperature, the microwave power input to the workchamber was increased to 3–4 kW. The temperature started increasing at rates measuring in thousands °C/min, and when it reached a preset maximum permissible temperature, the microwave power was turned off automatically and the samples cooled down freely. Examples of the temperature and the input microwave power records from these processes are shown in Figs. 1(a) and 1(b).

It can be seen that in the sintering process shown in Fig. 1(a), the time of temperature increase from 800 to 1400 °C is about 20 s. The average heating rate in this process is therefore about 1800 °C/min, and the maximum heating rate achieved immediately before the microwave power switch off is 4800 °C/min. After the microwave power switch off, the temperature does not fall down right away but continues to increase and then remains almost constant for a certain period of time. This temperature overshot, as discussed in Ref. [31], can result from the heat release produced by the solidification of the transient liquid phase that forms at the grain boundaries due to preferential absorption of the microwave radiation. At lower maximum temperatures and heating rates, this behavior is not pronounced [Fig. 1(b)], which suggests that the amount of the produced liquid phase is smaller but still sufficient for rapid densification.

The final density of all samples obtained in the processes with thermal instability at maximum temperatures 1305–1590 °C was in the range 98.1–98.9%. The microstructures of the obtained samples are shown in Figs. 2(a) and 2(b). The microstructures exhibit traces of the liquid phase and even localized regions of grain melting. However, even the sample obtained at a temperature as low as 1305 °C has uniform microstructure with fine grain size and low residual porosity [Fig. 2(b)].

Similar ultra-rapid microwave sintering processes were accomplished with Al_2O_3 samples. For example, in one of the experiments employing thermal instability, the maximum temperature was 1553 °C, the maximum input microwave power was 4.86 kW, and the maximum heating rate was 235 °C/min [Fig. 1(c)]. The process was carried out in air. The resulting relative density was 3.90 g/cm^3 (97.8%). It should be noted that an attempt to reproduce the same heating schedule using conventional heating (by introducing the sample manually into a preheated oven) resulted in a significantly lower density of the sintered material, 3.77 g/cm^3 (94.4%). The microstructure of the obtained samples exhibits rounded grains with an average size of about 0.5 μm [Fig. 2(c)].

The results described here, along with other similar experiments, suggest that the development of thermal instability

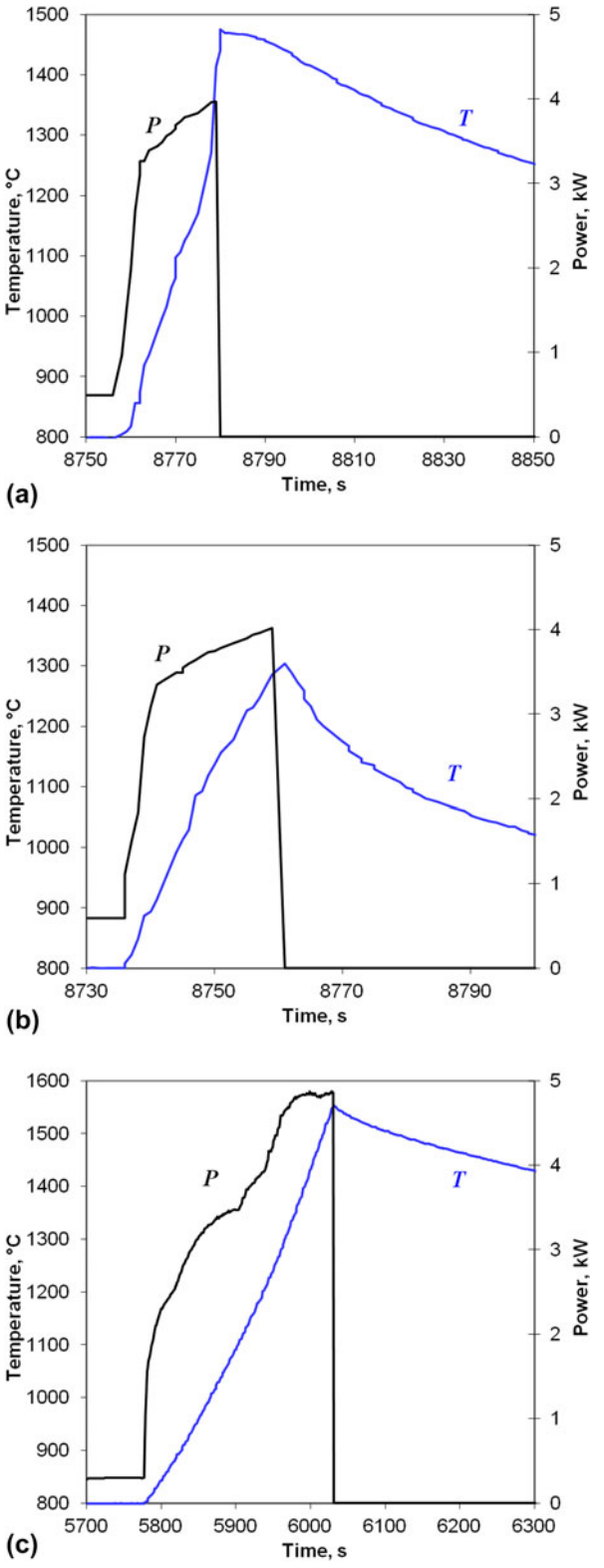


Figure 1: Temperature (*T*) and microwave power (*P*) input into the workchamber versus time, recorded at the high-temperature stage of the sintering processes using thermal instability: (a) Yb:$(LaY)_2O_3$—maximum temperature 1475 °C, maximum heating rate 4800 °C/min; (b) Yb:$(LaY)_2O_3$—maximum temperature 1305 °C, maximum heating rate 1000 °C/min; and (c) Al_2O_3—maximum temperature 1553 °C, maximum heating rate 235 °C/min.

https://doi.org/10.1557/jmr.2019.232 Published online by Cambridge University Press

© Materials Research Society 2019

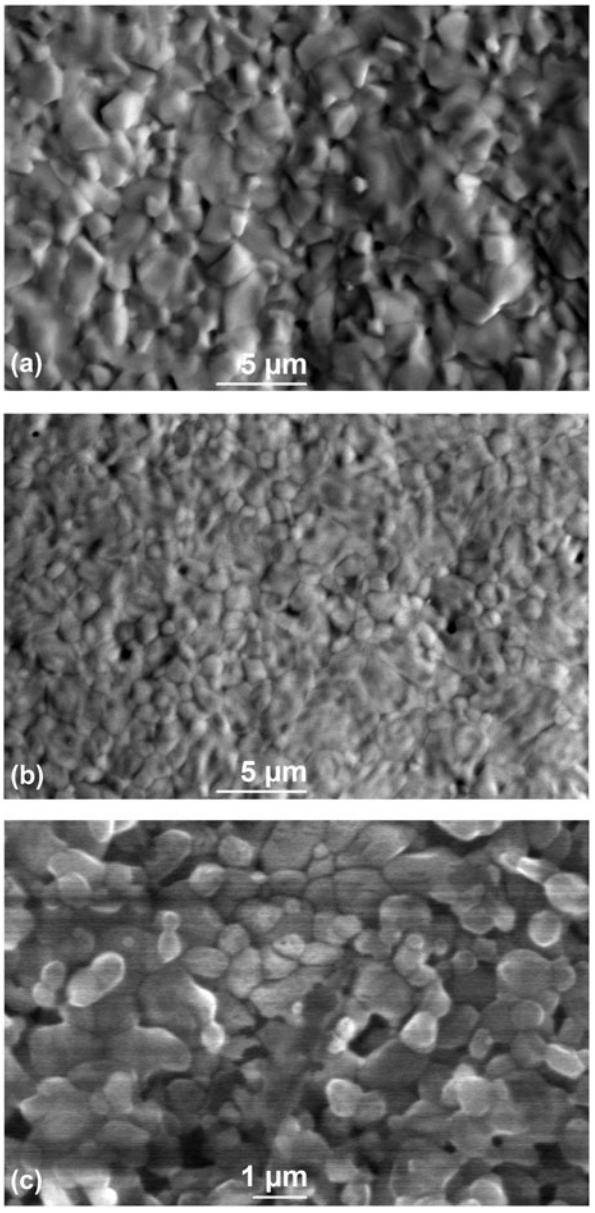


Figure 2: SEM images of unpolished surfaces of the samples sintered in ultra-rapid microwave processes with thermal instability: (a) Yb:$(LaY)_2O_3$—maximum temperature 1475 °C, maximum heating rate 4800 °C/min; (b) Yb:$(LaY)_2O_3$— maximum temperature 1305 °C, maximum heating rate 1000 °C/min; and (c) Al_2O_3—maximum temperature 1553 °C, maximum heating rate 235 °C/min.

occurs concurrently with a drastic increase in the mass transport rates in the material, resulting in ultra-rapid sintering that takes place in less than a minute's time. As will be discussed below, the physical mechanism responsible for both phenomena may involve softening of grain boundaries or even formation of a transient liquid phase, which leads to an enhancement in both mass transport and the microwave absorption properties. It should be noted that the volumetric heating by intense microwave radiation inevitably results in a significant temperature nonuniformity in the samples. Depending on the materials' properties, the temperature difference between the core and the periphery of the 13 mm diameter samples used in the experiments could be on the order of 100 °C even before the development of the thermal instability. Therefore, the onset and further development of thermal instability in different locations within the sample might occur at different instants of time. This leads to severe temperature gradients and nonuniform rapid densification, which in many cases deteriorates the properties of the final materials and sometimes even results in the loss of the samples' integrity. It should be noted here that the dog-bone-shaped samples commonly used for the demonstration of the DC field–assisted flash sintering effect typically have a cross-section of about 1×2 mm^2. The temperature nonuniformity may be insignificant in these laboratory experiments, but it poses a problem when attempts are made to scale them up [38, 39].

On the other hand, another approach that is pursued in the microwave processing of materials is based on the use of microwave radiation beams that can be focused into a spot with a size on the order of the electromagnetic wavelength [9]. The development of thermal instability in this case would further localize the heating and enhance densification. This opens prospects for the use of the described ultra-rapid microwave sintering method in developing applications for additive manufacturing of ceramics, employing higher-frequency millimeter-wave and terahertz radiation. First results on localized ultra-rapid consolidation of hydroxyapatite using 263 GHz radiation have been reported recently [40]. It has been demonstrated that using less than 100 W of millimeter-wave power focused into a spot with a cross-section area of about 2.5 mm^2, the hydroxyapatite powder could be brought to the melting temperature in several seconds. By scanning the millimeter-wave beam over the powder surface at a velocity on the order of 0.5 mm/s, extended densified hydroxyapatite structures have been obtained.

Ultra-rapid microwave sintering at constant heating rates with compensated thermal instability

In the microwave sintering experiments with many materials, it has been found necessary to limit the heating rate to prevent the nonuniform densification mentioned above while supplying a sufficient microwave power to activate the enhanced mass transport. This was implemented by employing automatic control over the microwave power using a feedback signal from the sensor measuring the temperature of the sample. In this manner, microwave heating could be carried out at a constant rate regardless of the changes in the material's absorptivity. In the experiments with 3% yttria-stabilized ZrO_2, it has been noted that sintering at higher heating rates can

https://doi.org/10.1557/jmr.2019.232 Published online by Cambridge University Press

© Materials Research Society 2019

result in obtaining dense ceramic material at lower temperatures. Figure 3 shows a comparison between the results of microwave heating at two different heating rates, 30 and 150 °C/min. It can be seen that at the higher heating rate near-full densities of the sintered materials could be obtained at sintering temperatures that are about 200 °C lower than those required for full densification at the lower heating rate. Further investigations have shown that for a given maximum temperature, the final density of 3% yttria-stabilized ZrO_2 obtained by microwave sintering increases with the increase in the microwave power absorbed per unit volume of material [34].

The effect of the absorbed microwave power has been also observed in the study of rapid microwave sintering of Al_2O_3 ceramics at constant heating rates. The dependencies of the final sintered density on the heating rate for several maximum sintering temperatures T_{max} are shown in Fig. 4. It can be seen that for lower maximum temperatures, an increase in the heating rate results in a noticeable decrease in the final sintered density. This phenomenon is typical of many non-isothermal sintering studies. The decrease in the density occurs because the effective sintering time becomes shorter with an increase in the heating rate. With an increase in the maximum temperature, the decrease in the final density is observed only for higher heating rates. For example, with T_{max} = 1350 °C, a decrease in the final density is observed for heating rates exceeding 50 °C/min, whereas for T_{max} = 1425 °C, the final density decreases noticeably when the heating rate exceeds 100 °C/min. For the maximum temperatures 1500 and 1600 °C, all the tested heating rates result in similar final densities.

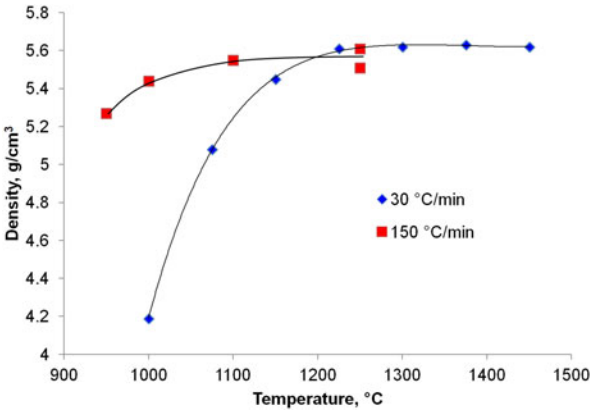


Figure 3: Density of the sintered samples versus maximum temperature for the microwave sintering of 3% yttria-stabilized ZrO_2 carried out at two heating rates, 30 and 150 °C/min, with no hold at maximum temperature.

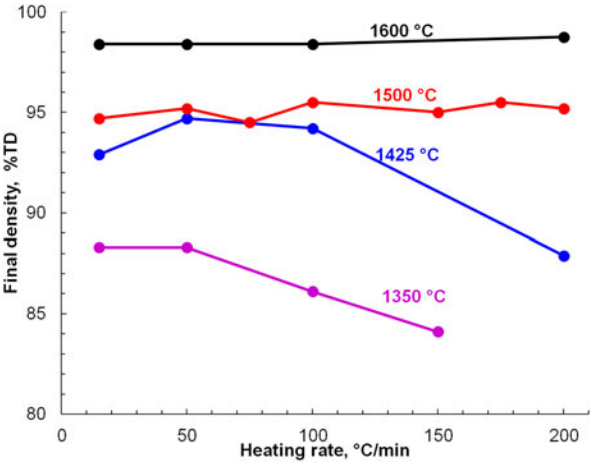


Figure 4: Density of the microwave sintered Al_2O_3 samples versus heating rate for four maximum temperatures of sintering T_{max} (zero hold time).

As discussed above, at higher levels of the volumetrically absorbed microwave power, the thermal instability develops in most ceramic materials. The automatic control over the input microwave power makes it possible to reduce the power immediately after the onset of thermal instability and thereby limits its further development while sustaining high heating rates. For efficient implementation of this functionality, it is important that the automatic control system is fast and provides wide dynamic range and high precision of the regulation of microwave power.

The implementation of the automatically controlled ultra-rapid sintering regimes will be discussed below taking Y_2O_3 and TiO_2 as example materials. Experiments with other materials such as Yb:$(LaY)_2O_3$ and $MgAl_2O_4$ have been described in detail elsewhere [31, 37].

The experiments with Y_2O_3 samples were carried out using a number of preset heating rates at the high-temperature stage of sintering (10, 25, 50, 100, and 200 °C/min) and maximum temperatures (in the range 1400–1700 °C) with no isothermal hold.

The time dependencies of the temperature of the sample (T_0), temperatures in the powder filling at distances 16 mm (T_1) and 35 mm (T_2) from the sample edge, and the microwave power input to the workchamber recorded in a sintering process with a heating rate of 25 °C/min and T_{max} = 1400 °C are shown in Fig. 5(a). It can be seen that at the high-temperature stage of heating (starting at $T_0 \approx 1050$ °C), the microwave power required to sustain the prescribed heating rate is approximately constant. This occurs in spite of the growing heat losses from the sample, which have radiative nature in the case of vacuum processing and hence are proportional to T_0^4. This fact evidences in favor of a strong dependence of the effective high-frequency electrical conductivity of Y_2O_3 on temperature.

The implementation of higher heating rates requires a corresponding increase in the automatically regulated microwave power. The elevated microwave power absorbed in the samples can trigger the development of thermal instability. Figure 5(b) shows the time dependencies of temperature and

https://doi.org/10.1557/jmr.2019.232 Published online by Cambridge University Press

© Materials Research Society 2019

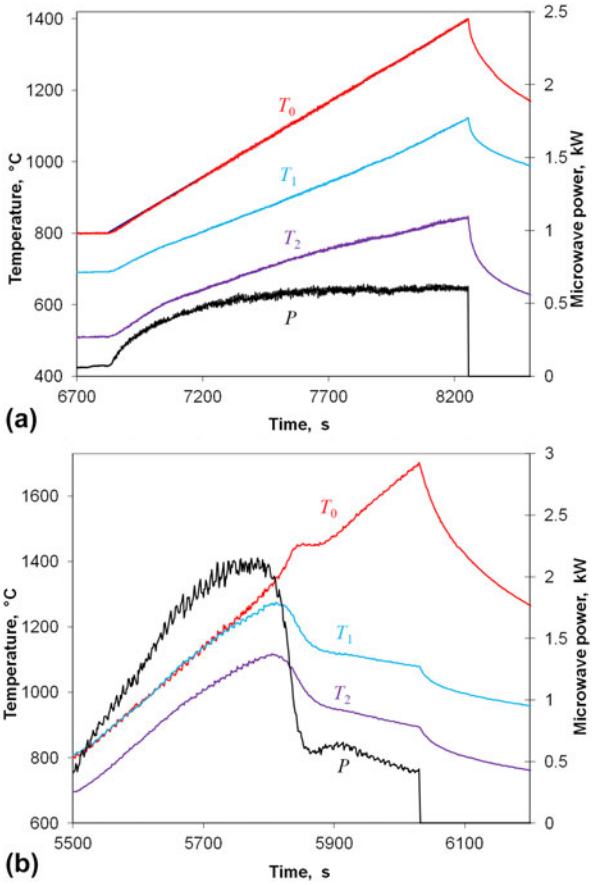


Figure 5: The temperature of the sample (T_0), temperatures in the powder filling at distances 16 mm (T_1) and 35 mm (T_2) from the sample edge, and the microwave power input to the workchamber versus time during the high-temperature stage of the sintering processes of Y_2O_3 samples: (a) with a heating rate of 25 °C/min and the maximum sintering temperature T_{max} = 1400 °C and (b) with a heating rate of 100 °C/min and the maximum sintering temperature T_{max} = 1700 °C.

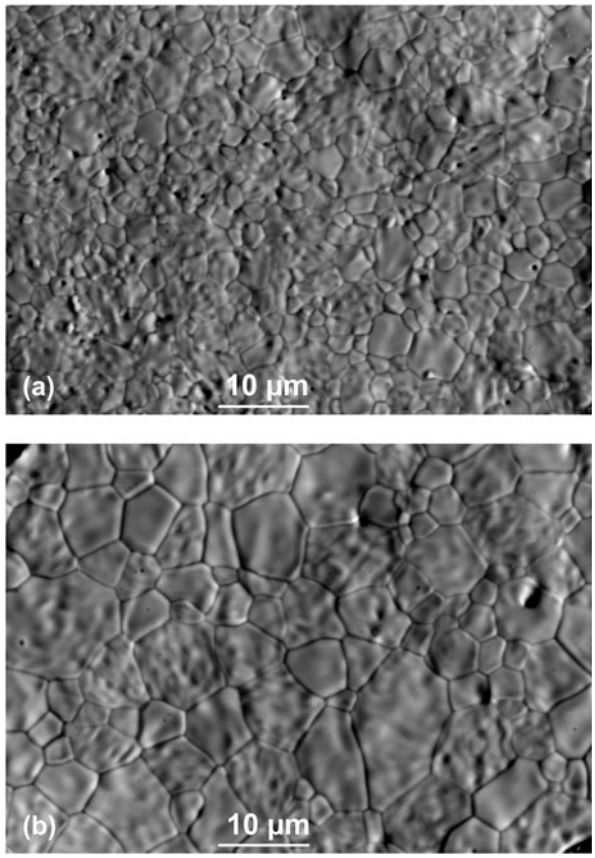


Figure 6: SEM images of the surfaces of the Y_2O_3 samples obtained in rapid microwave sintering processes with a heating rate of 100 °C/min: (a) maximum sintering temperature T_{max} = 1600 °C and (b) T_{max} = 1700 °C.

power recorded in a microwave sintering process with a preset heating rate of 100 °C/min and the maximum temperature of 1700 °C. It can be seen that at a temperature of about 1325 °C, the temperature growth begins to deviate from linear. This is obviously a manifestation of a thermal instability development. To compensate the temperature runaway, the automatic control system reduces the input microwave power sharply, which eventually results in the stabilization of the heating rate above $T_0 \approx 1425$ °C. The abrupt drop of the automatically regulated microwave power, actually being a signature of the thermal instability development, was observed in many experiments with different ceramic materials. As can be seen in Fig. 5(b), the reduction in the input microwave power caused a decrease in the temperatures T_1 and T_2 measured in the powder filling, while the temperature of the sample, T_0, continued to increase. A comparison with Fig. 5(a) suggests that although the microwave absorption in the powder filling could be considerable before the onset of thermal instability, upon its development the properties of the material of the sample change in such a way that the microwave absorption in it becomes much stronger than in the powder filling.

The microwave sintering experiments carried out at different heating rates in the range 50–200 °C/min have demonstrated that the onset temperature of thermal instability in Y_2O_3 samples does not depend on the heating rate (T_0 = 1325 ± 25 °C). Under the described experimental conditions, the maximum input power at the high-temperature stage of sintering (recorded before the onset of thermal instability) scaled approximately linearly with the heating rate. In the series with the maximum sintering temperature 1500 °C, the final density achieved in the processes with higher heating rates was consistently higher, varying from 88.2% at a heating rate of 50 °C/min to 96.0% at 200 °C/min [32], even though the effective sintering time decreased with the heating rate. This suggests that the development of thermal instability in the described experiments is associated with the sintering rate enhancement, and this enhancement is more pronounced at higher microwave power levels.

When the maximum temperature of the ultra-rapid microwave sintering processes was increased to 1600 and 1700 °C

Journal of Materials Research ■ Volume 34 ■ Issue 15 ■ Aug 14, 2019 ■ www.mrs.org/jmr

https://doi.org/10.1557/jmr.2019.232 Published online by Cambridge University Press

© Materials Research Society 2019

with zero hold time, samples with densities above 98% were obtained. The optimum heating rate was found to be 100 °C/min, leading to the highest final densities, 98.3 and 98.1%, for maximum process temperatures 1600 and 1700 °C, respectively. For comparison, the process with a slow heating rate of 10 °C/min to T_{max} = 1600 °C and a hold time of 15 min resulted in a lower final density, 97.6%.

The scanning electron microscopic (SEM) images of the microstructure of the Y_2O_3 samples sintered to densities above 98% are shown in Fig. 6. It can be seen that both intergranular and intragranular pores are present in the samples. The sample sintered in the process with T_{max} = 1600 °C [Fig. 6(a)] has a bimodal grain size distribution with the prevailing sizes 1–3 μm and 5–9 μm. The sample sintered in the process with T_{max} = 1700 °C [Fig. 6(b)] exhibits a much higher average grain size (~15 μm), in spite of the fact that its density is slightly lower. In many larger grains, there is an internal substructure with a characteristic dimension of about 1–3 μm. No any pronounced boundaries can be seen between the elements of this substructure, which suggests that it probably has formed by welding many micron-sized grains together. The microhardness of the Y_2O_3 samples obtained in rapid microwave sintering processes was 6.5–6.8 GPa, and the fracture toughness was 0.9–1.1 MPa·$m^{1/2}$.

Similar patterns of microwave power associated with the development of thermal instability have been observed in the experiments on ultra-rapid microwave sintering of TiO_2. Figure 7(a) shows the time dependencies of the temperature of the sample (T_0); the temperatures in the powder filling, T_1 and T_2; and the microwave power input to the workchamber for the heating process with a rate of 25 °C/min to T_{max} = 1100 °C.

It can be seen from Fig. 7(a) that the abrupt increase in the temperature during the heating of TiO_2 samples occurs even at moderate heating rates, and it is sharper than in the case of Y_2O_3 samples. The decrease in the automatically controlled microwave power associated with the thermal instability is also sharper. A comparison between the temperatures T_1 and T_2 measured in the powder filling during the sintering of TiO_2 (Fig. 7) and Y_2O_3 (Fig. 5) samples shows that the microwave radiation is absorbed much more intensely in TiO_2 than in Y_2O_3. For example, at a temperature of the samples T_0 = 1100 °C, the difference $T_0 - T_1$ is 670 °C in the case of TiO_2 and 200 °C in the case of Y_2O_3. Therefore, the temperature nonuniformity along the radius of the samples is also more pronounced in the case of TiO_2 samples.

At higher heating rates, the decrease in the automatically controlled microwave power at the onset of thermal instability is also sharper during the sintering of TiO_2 than in the case of Y_2O_3. Figure 7(b) shows the temperatures and the microwave power recorded during a microwave sintering process with a rate of 100 °C/min and T_{max} = 1100 °C. On the whole, the patterns of the automatically controlled microwave power evolution during the ultra-rapid sintering of TiO_2 samples are similar to those observed for Y_2O_3 samples at heating rates above 50 °C/min and maximum temperatures above 1500 °C.

The relative densities of the TiO_2 samples obtained in the microwave sintering processes with different heating rates were in the range 91.5–94.8%, with an average of 93.1%. Similar to the above discussed experiments, they almost did not depend on the heating rate. Insignificant deviations from the average value could be caused by the difference in the initial densities of the green samples.

The evolution of the automatically controlled microwave power observed in the above described experiments, as well as in similar experiments with other materials such as Yb:$(LaY)_2O_3$ [31] and $MgAl_2O_4$ [37], can be explained as follows [31, 35]. The microwave power absorbed in a sample increases its temperature and/or compensates the heat losses:

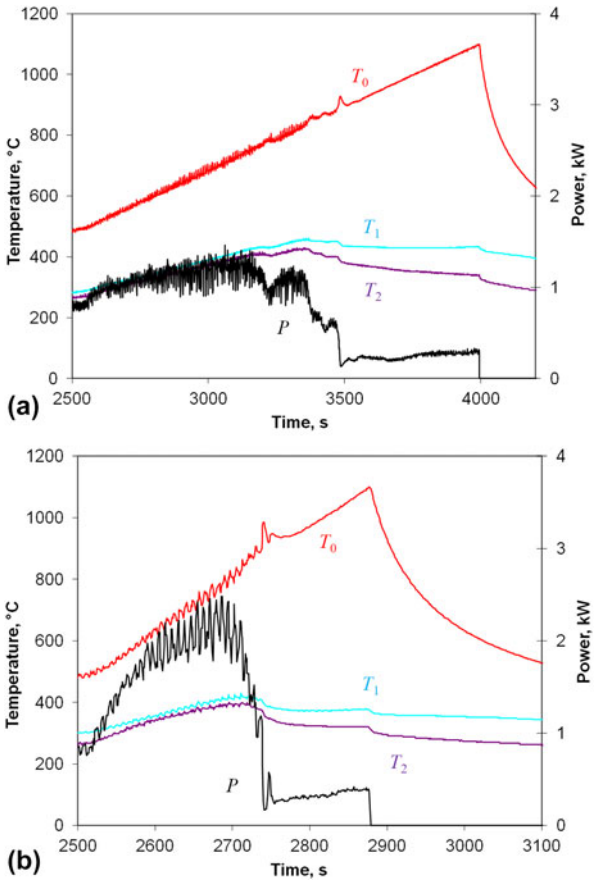


Figure 7: The temperature of the sample (T_0), temperatures in the powder filling at distances 16 mm (T_1) and 35 mm (T_2) from the sample edge, and the microwave power input to the workchamber versus time during the high-temperature stage of the sintering process of a TiO_2 sample with the maximum sintering temperature T_{max} = 1100 °C and a heating rate of (a) 25 °C/min and (b) 100 °C/min.

https://doi.org/10.1557/jmr.2019.232 Published online by Cambridge University Press

© Materials Research Society 2019

$$p_{abs} = \rho C \frac{dT}{dt} + p_{hl} \quad , \tag{1}$$

where p_{abs} is the microwave power absorbed per unit volume of the sample, ρ is density, C is specific heat capacity of the material of the sample, dT/dt is the heating rate, and p_{hl} is the power in heat losses. In general, p_{hl} is the total power lost by thermal conductivity, convection, and thermal radiation. The power in heat losses increases as the temperature of the sample grows. Therefore, during constant rate heating, the microwave power absorbed per unit volume of the sample, p_{abs}, increases monotonically (unless there are phase transformations accompanied with the changes in the internal energy of the sample), as shown in Fig. 8(a).

The characteristic values of the microwave power absorbed per unit volume of the sample, p_{abs}, can be estimated from the energy balance equations using the data on the heating and the cooling rates recorded immediately before and after the time instant when the maximum temperature is reached [31]. These values depend on factors such as the selected heating schedule, microwave absorbing properties of the specific materials, and thermal insulation conditions. For example, the following maximum values of p_{abs} have been determined in the experiments on ultra-rapid microwave sintering: p_{abs} = 20–160 W/cm^3 for Yb:$(LaY)_2O_3$ ceramics [33], p_{abs} = 15–100 W/cm^3 for Al_2O_3 [33], p_{abs} = 60–120 W/cm^3 for 3YSZ [34], p_{abs} = 40–43 W/cm^3 for Y_2O_3 [35], p_{abs} = 27–80 W/cm^3 for $MgAl_2O_4$ [37], etc. It should be noted that the power density of Joule heating required for the onset of the flash sintering in the DC field-assisted experiments with various materials has the same order of magnitude, 10–100 W/cm^3 [41].

The power p_{abs} absorbed per unit volume of the sample [Eq. (1)] is equal to the product of the square of the electric field strength in the sample, E_s^2, and the effective high-frequency electric conductivity of the material of the sample, σ:

$$p_{abs} = \sigma E_s^2 \quad . \tag{2}$$

Unlike the DC field–assisted flash sintering, in the microwave sintering experiments it is not possible to directly measure the power absorbed in the volume of the sample. However, the microwave power input to the workchamber, P_{input}, is being measured throughout the microwave sintering process.

The workchamber of the gyrotron system is an untuned multimode cavity [42] with a high ratio of its volume, V, to the cube of the radiation wavelength, λ: $V/\lambda^3 \approx 10^5$. In such a cavity, the electromagnetic field distribution over the volume is quasi-uniform because it comprises a superposition of many oscillation modes excited simultaneously [43]. The quality

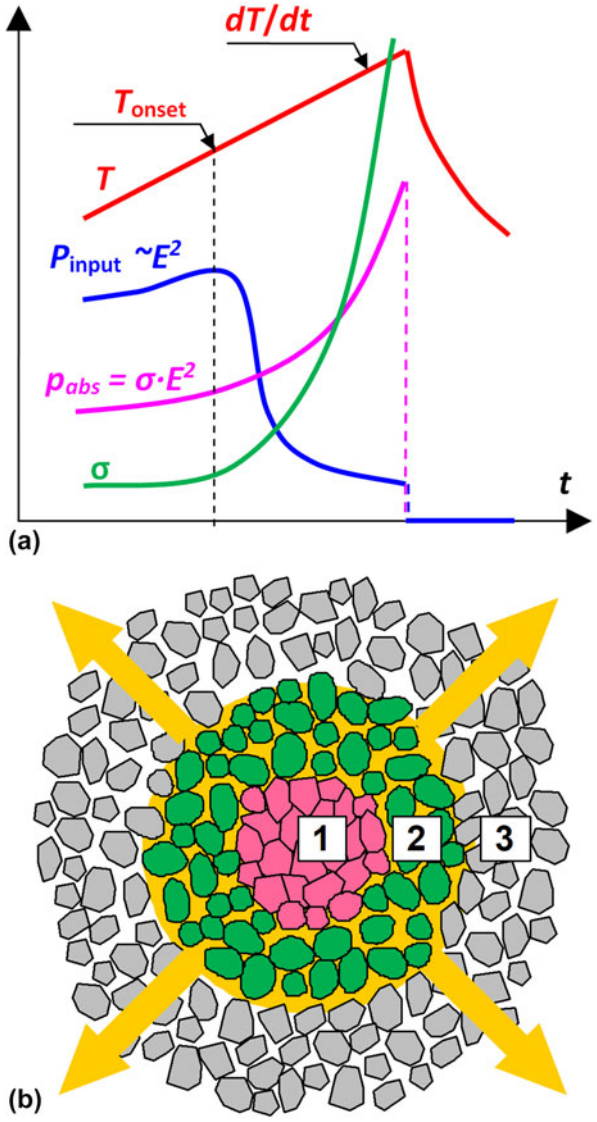


Figure 8: Schematic illustrations to the mechanism of ultra-rapid microwave sintering: (a) microwave power absorbed per unit volume of the sample, p_{abs}; input microwave power recorded during an ultra-rapid microwave sintering process, P_{input}; and the effective conductivity of the sample, σ, versus time during microwave heating at a constant rate dT/dt; and (b) propagation of a densification front in the ceramic powder compact: 1—sintered core region; 2—region with rounded grains surrounded by liquid phase (note that this is also the region of maximum volumetric power deposition); 3—unsintered peripheral region awaiting arrival of the densification front.

factor, Q, for this type of cavity is determined primarily by the Ohmic losses in its walls and can be estimated easily [44]. The input power, P_{input}, determines the magnitude of the electromagnetic energy, W, stored in the cavity [45]:

$$W = \frac{Q}{\omega} P_{input} = \varepsilon_0 \int E^2 dV \approx \varepsilon_0 E^2 V \quad , \tag{3}$$

where ω is the microwave cyclic frequency, ε_0 is the electric constant, E is the electric field strength in the cavity, and V is the volume of the workchamber. The electric field strength, E_s,

https://doi.org/10.1557/jmr.2019.232 Published online by Cambridge University Press

© Materials Research Society 2019

in a small sample placed in the cavity is approximately equal to the electric field strength in the cavity outside of the sample: $E_s \approx E$. Then, expressing E^2 from Eq. (3) and substituting to Eq. (2), it is easy to obtain the interrelation between the high-frequency electric conductivity of the ceramic material, σ, the power incoming the workchamber, P_{input}, and the microwave power absorbed per unit volume of the sample, p_{abs}:

$$\sigma \approx \frac{\varepsilon_0 \omega V}{Q} \frac{p_{abs}}{P_{input}} \quad . \tag{4}$$

According to Eq. (4), the effective conductivity is at any instant of time proportional to the ratio of the microwave power absorbed per unit volume of the sample and the input microwave power supplied to the workchamber. Since p_{abs} is a growing function of temperature as discussed above, the abrupt decrease in the input microwave power, P_{input}, in a constant rate heating process necessarily means an even sharper increase in the effective conductivity of the ceramic material.

The quantitative estimates accomplished for the ultra-rapid microwave sintering process of Yb:$(LaY)_2O_3$ ceramics [31] demonstrate that in the course of the thermal instability development, the effective conductivity approaches the values that are characteristic of the melt phase of the material. The in situ measurements of DC electric conductivity during microwave heating [36] have demonstrated that its temperature dependence deviates from the Arrhenius law at high levels of the microwave power, which indicates that the phase state of the material is changed and a highly electrically conductive phase is formed in the sample. Along with the results of microstructure studies, which show traces of the liquid phase extruded at the grain boundaries of the sintered samples [31, 33], the protruding edges of the grains formed due to their softening [33], and different elemental composition of the intragranular and intergranular phases [33], this suggests that the liquid phase plays an important role in the mechanism responsible for rapid densification. This appears to be in line with the proposed mechanisms of enhanced densification in DC field–assisted flash sintering processes that involve grain boundary melting of softening and transient liquid phase formation [46, 47, 48].

The mechanism of ultra-rapid sintering proposed by Bykov et al. [33] is equally applicable to both microwave and DC field–assisted processes as long as they rely on volumetric heating—either due to microwave absorption or due to Joule heat released by the DC electric current. According to this mechanism, the principal stages of the ultra-rapid sintering process can be described as follows [Fig. 8(b)]:

(i) the volumetric heating creates a nonuniform temperature distribution in which the interior of the sample is the hottest;
(ii) the liquid phase begins to form at particle surfaces, which are sites of preferential energy deposition. The temperature required for this can be lower than the bulk melting temperature of the material due to the elevated concentration of defects and impurity atoms at the particle surfaces;
(iii) liquid films surround particles and facilitate mass transport. The particle shape becomes rounded, and particles rotate and slide relative to each other;
(iv) upon local completion of rapid densification, the liquid phase is squeezed from the interior toward the periphery of the sample. In the densified core region, the development of local thermal runaway is terminated, preventing the destruction of the sample;
(v) the region of maximum power deposition (which coincides with the predominant location of the liquid phase due to its elevated effective conductivity) also moves outwards;
(vi) the propagation of the described densification front results in achieving full density throughout the entire sample (along with a concurrent grain growth).

The preliminary results of in situ optical dilatometry studies during rapid microwave sintering of Al_2O_3 ceramic samples indicate that at higher levels of microwave power, there is an increase in the shrinkage rate, which occurs concurrently with the development of thermal instability [49]. Work is underway to investigate the dynamics of the temperature distribution in the sample in its interplay with the enhanced densification by in situ infrared imaging.

Ultra-rapid microwave sintering of metal powders using resonant absorption

The ultra-rapid sintering processes based on the thermal instability normally cannot be implemented with powder metals because the electrical conductivity of metal decreases with an increase in temperature. Recent studies have demonstrated that rapid microwave heating of metal powders can be possible due to resonant absorption phenomena.

Microwave sintering of metal powder compacts has been actively investigated during the last two decades by many research teams, starting from the pioneering study by Roy et al. [50]. The ability of metal particles to heat under microwave irradiation is in most cases associated with the release of Joule heat by eddy electric currents induced by the alternating magnetic component of the microwave field. The energy losses in metal powders can therefore be expressed by an imaginary part of the effective magnetic permeability of the material. However, this interpretation is essentially a result of simplification because it implicitly assumes that the magnetic field in the metal particle can be considered spatially uniform, giving

https://doi.org/10.1557/jmr.2019.232 Published online by Cambridge University Press

© Materials Research Society 2019

rise to purely rotational electric field by virtue of Maxwell's equations. The estimates show that for higher frequencies and higher conductivities of metal this is not necessarily the case, since the wavelength in the metal can be comparable or even smaller than the particle size. In this case, both the electric and the magnetic components of the field inside the particle contribute to energy losses.

The response of powder materials to the electromagnetic field is determined by the effective dielectric and magnetic properties, which can be calculated within various approximate models taking into account the composition, size, and shape of the particles (see, e.g., [51], for a brief review). In particular, models based on the effective medium approximation originally proposed by Bruggeman [52] are especially appropriate for the description of the materials' properties during sintering, when the volumetric ratio of components (solid and void phases) can change in a broad range. With respect to electrically conductive powders, it has been shown by the authors that they can exhibit considerable microwave absorption in the case when the particles are surrounded by insulating layers (e.g., native oxide) [53]. Recently, these results have been generalized into the case of well-conducting metals in higher-frequency microwave fields. As a result, equations for the effective dielectric permittivity ε_{eff} of compacted metal powders have been obtained by advancing the effective medium approximation beyond the quasi-electrostatic limit [54]. Using a similar method, equations for the effective magnetic permeability μ_{eff} of these materials have also been obtained [55].

An important role of the native oxide layers in the character of microwave absorption during microwave sintering of powder metals has been demonstrated experimentally [56, 57]. The results of modeling have shown that the powder materials in which the electrically conductive particles are separated by thin insulating layers have low values of both dielectric and magnetic loss tangents, $\tan \delta_e = \mathrm{Im}\ \varepsilon_{eff}/\mathrm{Re}\ \varepsilon_{eff}$ and $\tan \delta_m = \mathrm{Im}\ \mu_{eff}/\mathrm{Re}\ \mu_{eff}$ [53, 58]. In effect, such metal powders respond to the microwave field in a way that is similar to low-loss dielectrics. Therefore, they can exhibit resonant absorption when exposed to microwaves, which can be used to implement rapid microwave heating and sintering [58]. The resonance effects leading to extremely rapid densification have been observed in the experiments on microwave sintering of titanium-based metal powders [59].

In general, simulation of microwave sintering is a so-called multiphysics task that includes solutions of the electromagnetic problem and the thermal problem and models of the densification, grain growth, and mechanical stresses [11]. A simple semianalytical model that describes the ultra-rapid microwave sintering of metal powders has been suggested in Ref. [58]. It includes an analytical electrodynamic solution for a spherical powder compact irradiated by a plane wave [60], an energy balance equation to account for the volumetric power deposition and heat losses, and a model of densification based on the master sintering curve approach [61]. The temperature- and density-dependent effective dielectric and magnetic properties of the compacted metal powder are calculated at each iteration of the simulation within the non-static effective medium approximation [54, 55].

Some examples of the ultra-rapid microwave sintering processes of titanium powder compacts simulated using the model developed in Ref. [58] are shown in Fig. 9. In all cases, the intensity of the incident microwave radiation was taken constant. In Fig. 9(a), it can be seen that the heating of a compact at first saturates at a temperature not exceeding 600 °C, at which the densification is quite slow. After approximately 500 s, when the relative density increases by about 3% of the initial value (50%), the temperature suddenly grows sharply in several steps, and the sample is rapidly sintered to a density of about 90% in approximately 30 s time. Then, the temperature returns down to about 600 °C and the densification stalls.

The explanation of this evolution of the temperature and density lies in the resonance phenomenon. The resonance occurs when the diameter of the spherical sample d is approximately an integer multiple of half-wavelength of the electromagnetic radiation in the material of the sample. The wavelength λ is determined by the radiation frequency ω and the dielectric and magnetic properties of the material: $\lambda = 2\pi c/\left(\omega \mathrm{Re}\sqrt{\varepsilon_{eff}\mu_{eff}}\right)$, where c is the velocity of light. Since the response of the metal particles to the electromagnetic field is associated with the generation of electric currents, both the effective dielectric permittivity ε_{eff} and the magnetic permeability μ_{eff} of the powder material are determined by the electrical conductivity of metal, which is temperature dependent. In addition, the effective properties depend on the volumetric ratio of the components in the mix (solid and void phases), and hence, they change with the increase in the relative density of the compact during sintering. On the other hand, the increase in the density causes shrinkage of the sample and therefore its diameter also changes. Therefore, the diameter to half-wavelength ratio, $2d/\lambda$, changes throughout the sintering process. In the example shown in Fig. 9(a), the calculations indicate that the slow evolution of the density brings the sample to resonance with $2d/\lambda \approx 11$ at $t = 494$ s. The power absorption peak associated with the resonance results in a sharp increase in the temperature, which causes rapid densification. The strong changes in both the temperature and density lead to variations in the effective dielectric properties and hence in the value of the electromagnetic wavelength in the compacted powder material. As a result, within a short time, the sample passes through a sequence of resonance absorption peaks with $2d/\lambda$ equal to integer numbers from 11 to 15.

https://doi.org/10.1557/jmr.2019.232 Published online by Cambridge University Press

© Materials Research Society 2019

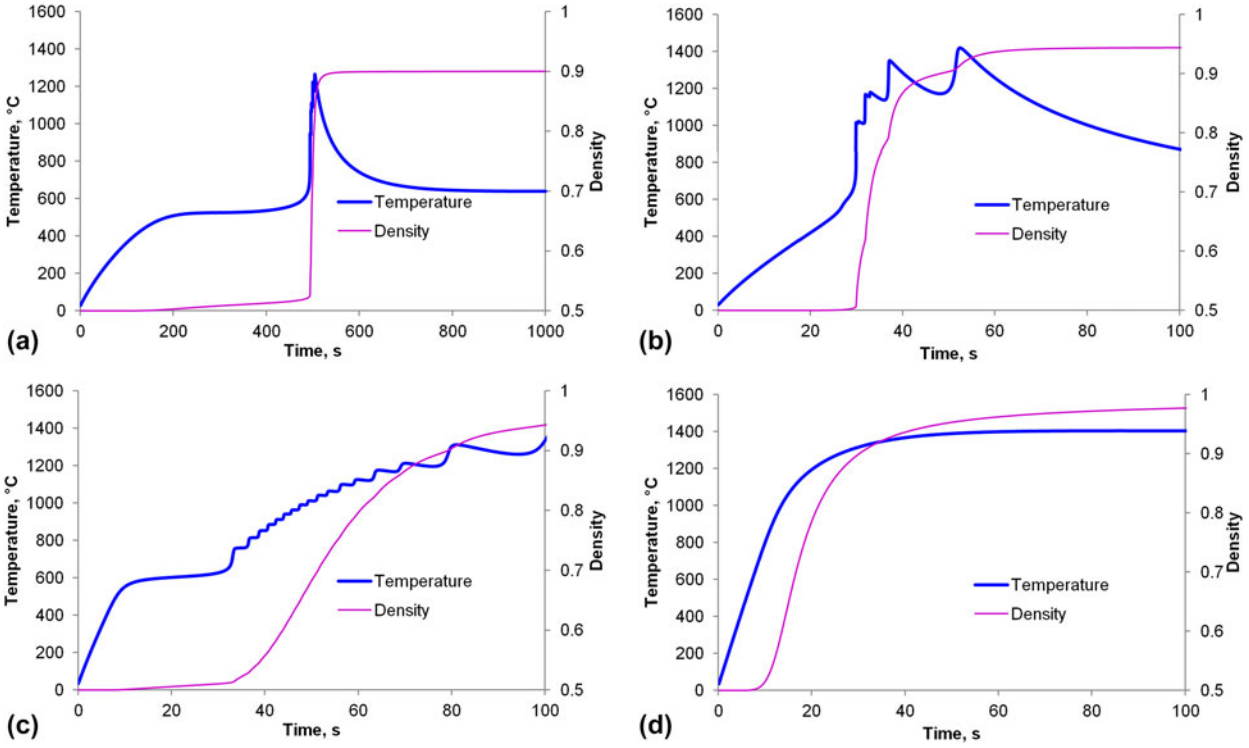


Figure 9: Simulated evolution of the temperature and relative density of a spherical titanium powder compact irradiated by a plane electromagnetic wave with a constant intensity: (a) initial diameter of the sample $d_0 = 2$ cm, microwave frequency $f = 2.45$ GHz; (b) $d_0 = 1.904$ cm, $f = 2.45$ GHz; (c) $d_0 = 6$ cm, $f = 2.45$ GHz; and (d) $d_0 = 2$ cm, $f = 24$ GHz. Simulation parameters: microwave intensity 800 W/cm^2, initial relative density of compacts 50%, particle radius 1 μm, and thickness of oxide layer on the particle surface 2.5 nm. Master sintering curve data from [66].

By adjusting the initial diameter of the metal powder compact closer to one of the "resonant" values, it is possible to significantly shorten the wait time before sharp densification occurs. For example, the initial diameter of the compact simulated in Fig. 9(b) was chosen close to 5λ, which has made it possible to provide close-to-resonant absorption conditions right away from the process start and obtain the final density in excess of 94% in less than 100 s. The process simulated in Fig. 9(b) passes through six resonance absorption peaks with $2d/\lambda$ equal to integer numbers from 10 to 15 (the first two peaks in the temperature curve overlap because they are separated by a time interval of only 0.5 s). It can be seen in the density curve that the densification advances with each resonance absorption peak.

To stabilize the heating rate for an arbitrary initial diameter of the sample, it would be advisable to increase the diameter to half-wavelength ratio, so that there would be multiple resonance absorption peaks with the overlapping responses of the sample temperature to them. The diameter of the compact simulated in Fig. 9(c) is three times larger than that in Fig. 9(a). During the sintering process, it passes through 18 resonance absorption peaks with $2d/\lambda$ equal to integer numbers from 32 to 49. In this case, small steps are only visible in the temperature curve, and the densification curve is quite smooth.

Another implementation of the same approach would be to increase the microwave frequency. Figure 9(d) shows a simulated sintering process of a sample with the same initial diameter as in Fig. 9(a) but carried out at a frequency of 24 GHz rather than 2.45 GHz. The corresponding increase in the diameter to half-wavelength ratio makes it possible to implement a very efficient microwave heating process and to achieve almost full densification in an even shorter time.

Another method suggested in Ref. [58] to provide efficient resonant microwave absorption throughout the sintering process is to use a variable frequency microwave source and adjust its frequency continuously, so that the resonance would be sustained at all times. Due to the presence of multiple resonances, it would be sufficient in most cases to tune the frequency in a narrow range, with a relative bandwidth on the order of several percent, "jumping" from one resonance to another as the frequency approaches the edge of the band. It should be noted that although the model developed in Ref. [58] considers the analytically solvable case of spherical powder compacts, resonant absorption peaks would be as well present during the microwave heating of compacts of other shapes.

The presence of partial interparticle connectivity in the metal powder (due to disrupted oxide films, particle surface roughness, etc.) decreases the Q-factor and makes the resonant

https://doi.org/10.1557/jmr.2019.232 Published online by Cambridge University Press

© Materials Research Society 2019

absorption peaks not so sharp. In this case, a fraction of the total absorbed microwave power remains in the form of Joule heat in the metal, whereas the remainder is released in the interparticle contacts. It has been demonstrated that the ultra-rapid resonant microwave sintering is still feasible in this case at least until the contribution of the interparticle contacts into the absorption does not exceed the contribution of Joule losses in the particles [62]. A similar model can be employed in this case to calculate the effective dielectric properties of the powder material, with an addition of an imaginary part to the dielectric constant of the material of the oxide layers surrounding the particles. The effective electrical conductivity of the material of the layers that gives rise to this imaginary part can be derived from the experimentally measureable macroscopic conductivity of the compacted powder samples [62].

Conclusion

Microwave heating offers an opportunity to implement ultra-rapid sintering processes of both ceramic materials and powder metals, as well as various composite materials. The conditions that should be met to achieve this goal are (i) to ensure efficient absorption of the electromagnetic energy in the material and (ii) to activate mechanisms of enhanced mass transport.

It has been demonstrated that in oxide ceramic materials both these conditions can be fulfilled via a controlled development of the thermal instability during the volumetric microwave heating. The sharp increase in the effective conductivity of the material leading to the instability is associated with the softening of the powder particle surfaces and formation of transient liquid phase, which serves as a path for fast mass transport and promotes ultra-rapid densification. The region of maximum microwave absorption coincides with the location of liquid phase formation. Due to the inverse temperature distribution arising in the processes of volumetric microwave heating, the densification would start in an inner part of the sample and rapidly propagate as a front toward its periphery.

The implementation of ultra-rapid microwave sintering processes requires fast and precise control over the microwave power, based on the temperature signal or other process variables. Ultra-rapid microwave sintering has been accomplished on a number of oxide ceramic materials using two kinds of processing regimes. In one case, the samples were exposed to microwave radiation of fixed intensity, and the thermal instability was allowed to develop until a preset maximum permissible temperature was reached. Within another approach, the microwave power was regulated continuously to implement preset temperature–time schedules with high rates of heating. The onset of thermal instability manifests itself as a sharp decrease in the automatically regulated microwave power.

Ceramic samples sintered to virtually full density have been obtained by ultra-rapid microwave sintering. The materials have uniform microstructures and exhibit competitive mechanical and functional properties. An advantage of using microwave heating for rapid consolidation is that this method does not require electrodes to supply the electromagnetic energy to the material. This makes ultra-rapid microwave sintering a promising approach for developing novel applications for consolidation of ceramics, including additive manufacturing technologies.

Microwave ultra-rapid sintering of metal powders and metal–ceramic composites can be implemented using resonant absorption of microwave radiation. Simulations demonstrate that high efficiency of microwave heating can be achieved in such materials, which would result in their densification within similar process times as those demonstrated in the ultra-rapid microwave sintering of ceramic samples.

Methodology

The experiments on ultra-rapid microwave sintering were carried out using gyrotron systems for high-temperature microwave processing of materials [44, 63]. The source of microwave radiation is a gyrotron operating at a frequency of 24 GHz with an output microwave power of 6 kW. The microwave radiation from the gyrotron is fed into the workchamber, which has a cylindrical shape with a diameter of 50 cm and a height of 60 cm. The workchamber is equipped with a mode-stirring device for improving the homogeneity of the electromagnetic field distribution.

The output power of the gyrotron is regulated by a control system continuously in the range from zero to maximum. The temperature of the samples is monitored with a sampling rate of 1–10 s^{-1} and compared with the preset temperature–time schedule. The difference signal is used to control the output voltage of the high-voltage power supply according to a proportional–integral–derivative (PID)-type algorithm developed purposely for this system. In the experiments described below, unshielded B-type thermocouples were used as temperature sensors. In most of the experiments, the thermocouple head was inserted into a small hole drilled to the center of the sample. In this manner, the maximum temperature was measured, which is achieved in the center of the sample under conditions of volumetric microwave heating. The thermocouple signals were calibrated according to the procedure described in Ref. [64]. The accuracy of temperature measurements in the range 1000–1600 °C is within ±10 °C.

The temperature measurement and data acquisition system has been purposely optimized to control ultra-rapid heating processes. The system is capable of sustaining temperature–time schedules of any kind. In most of the experiments, the

https://doi.org/10.1557/jmr.2019.232 Published online by Cambridge University Press

© Materials Research Society 2019

TABLE I: Powders and compaction methods used for the preparation of the experimental samples.

Powder composition	Supplier or synthesis method	Particle size information	Method of compaction	Green density of compacts
Al_2O_3 (+0.05% MgO)	AES-11C, Sumitomo Chemical Co., Ltd., Japan	D_{50} = 0.45 μm	Slip casting + cold isostatic pressing at 150 MPa	64%
ZrO_2 (+3% Y_2O_3)	TZ-3Y, Tosoh Corporation, Japan	Crystallite size—27 nm, particle size (D_{50})—0.6 μm, specific surface area—16 m^2/g	Slip casting	49.5%
TiO_2	Nanophase Technologies, USA; converted to rutile by annealing at 900 °C	Mean particle size 34 nm (initial anatase powder); coherent scattering domain size 76 nm (rutile)	Uniaxial pressing at 200–300 MPa	50%
Y_2O_3	Produced by self-propagating high-temperature synthesis [65]	Brunauer–Emmett–Teller (BET) particle size 130 nm; average agglomerate size 15 μm	Uniaxial pressing at 200–300 MPa	42%
5 at.% Yb:$(La_{0.1}Y_{0.9})_2O_3$	Prepared via a wet chemical route from a mixture of commercial Y_2O_3, La_2O_3, and Yb_2O_3 powders (all 99.99% pure) [31]	Specific surface area 8 m^2/g (BET)	Uniaxial pressing at 400 MPa	52%

samples were first brought to an intermediate temperature (usually 800 °C) and held at this temperature for about 1 h to remove residues of organic binders and the absorbed water. No densification of the samples was detected at this stage. Then, if vacuum sintering was required, the workchamber was evacuated to 1–10 Pa, and the samples were heated to the preset target temperature at an automatically sustained constant (or slowly varying) heating rate in the range 10–200 °C/min. There was no isothermal hold at the target temperature. In the experiments with uncontrolled temperature instability, the microwave power was set manually, and the automatic control system only switched the power off on reaching a preset maximum permissible temperature.

Either commercially available or individually synthesized ceramic powders were used for sample preparation. The information about the powders and compaction methods used in the described experiments is listed in Table I. The compacted samples in all cases had a pellet shape with a diameter of 12–13 mm and a thickness of 2.5–3 mm.

In most of the described experiments, the compacted samples were positioned in the center of a cylindrical quartz crucible, 100 mm in diameter and 100 mm in height. To thermally insulate the samples, the crucible was filled with either coarse (particle size 3–5 μm) Y_2O_3 powder (in the case of Yb:$(LaY)_2O_3$, Y_2O_3, and TiO_2 samples) or coarse alumina powder (Al_2O_3 and ZrO_2 samples). In the experiments with Y_2O_3 and TiO_2 samples, additional thermocouples were positioned in the powder filling at distances 16 and 35 mm from the sample edge to characterize the temperature distribution and determine the direction of the heat flux. To vary the thermal insulation conditions and hence the level of the microwave power required for the heating of the samples to a given temperature, in some cases the samples were placed in a rectangular container made of plates of highly porous, low microwave absorbing material (Valox-1750; Thermoceramica Ltd., Khimki, Russia).

The density of the sintered samples was determined by Archimedes weighing in distilled water with an estimated accuracy of ±0.01 g/cm^3. The microstructure was studied on unpolished side surfaces and fracture surfaces of the as-sintered samples by SEM (JEOL JSM-6390 LV, JEOL Ltd., Akishima, Tokyo, Japan). The grain structure profiles were investigated by atomic force microscopy (Smena, NT-MDT, Moscow, Russia). The phase composition of the sintered samples was analyzed by X-ray diffractometry (Rigaku Ultima IV, Rigaku Corporation, Tokyo, Japan).

Acknowledgments

This research was supported in part by Russian Science Foundation, Grant No. 17-19-01530 (ultra-rapid microwave sintering of ceramic materials and powder metals), and Russian Foundation for Basic Research, Grant No. 18-29-11045 (the development of an additive manufacturing method based on ultra-rapid millimeter-wave sintering).

References

1. **W.R. Tinga and W.A.G. Voss**: *Microwave Power Engineering* (Academic Press, New York, New York, 1968).
2. **A.J. Berteaud and J.C. Badot**: High temperature microwave heating in refractory materials. *J. Microwave Power* **11**, 315 (1976).
3. **J.M. Osepchuk**: A history of microwave heating applications. *IEEE Trans. Microwave Theory Tech.* **32**, 1200 (1984).
4. **T.T. Meek, C.E. Holcombe, and N. Dykes**: Microwave sintering of some oxide materials using sintering aids. *J. Mater. Sci. Lett.* **6**, 1060 (1987).
5. **D.L. Johnson**: Microwave and plasma sintering of ceramics. *Ceram. Int.* **17**, 295 (1991).
6. **W.H. Sutton:** Microwave processing of ceramics—An overview. In *Microwave Processing of Materials III*, R.L. Beatty, W.H. Sutton, and M.F. Iskander, eds.; Materials Research Society Symposium Proceedings, Vol. **269** (Materials Research Society, Pittsburgh, Pennsylvania, 1994); p. 3.

https://doi.org/10.1557/jmr.2019.232 Published online by Cambridge University Press

© Materials Research Society 2019

7. **J.D. Katz**: Microwave sintering of ceramics. *Annu. Rev. Mater. Sci.* **22**, 153 (1992).
8. **D.K. Agrawal**: Microwave processing of ceramics: A review. *Curr. Opin. Solid State Mater. Sci.* **3**, 480 (1998).
9. **Y.V. Bykov, K.I. Rybakov, and V.E. Semenov**: High-temperature microwave processing of materials. *J. Phys. D: Appl. Phys.* **34**, R55 (2001).
10. **J.G.P. Binner and B. Vaidhyanathan**: Microwave sintering of ceramics: What does it offer? *Key Eng. Mater.* **264–268**, 725 (2004).
11. **K.I. Rybakov, E.A. Olevsky, and E.V. Krikun**: Microwave sintering—Fundamentals and modeling. *J. Am. Ceram. Soc.* **96**, 1003 (2013).
12. **J.A. Eastmen, K.E. Sickafus, J.D. Katz, S.G. Boeke, R.D. Blake, C.R. Evans, R.B. Schwarz, and Y.X. Liao:** Microwave sintering of nanocrystalline TiO_2. In *Microwave Processing of Materials II*, W.B. Snyder, Jr., W.H. Sutter, M.F. Iskander, and D.L. Johnson, eds.; Materials Research Society Symposium Proceedings, Vol. **189** (Materials Research Society, Pittsburgh, Pennsylvania, 1990); p. 273.
13. **J. Freim, J. McKittrick, J. Katz, and K. Sickafus**: Microwave sintering of nanocrystalline γ-Al_2O_3. *Nanostruct. Mater.* **4**, 371 (1994).
14. **Y. Bykov, A. Eremeev, S. Egorov, V. Ivanov, Y. Kotov, V. Khrustov, and A. Sorokin**: Sintering of nanostructural titanium oxide using millimeter-wave radiation. *Nanostruct. Mater.* **12**, 115 (1999).
15. **G. Roussy and J. Mercier**: Temperature runaway of microwave heated materials: Study and control. *J. Microwave Power* **20**, 47 (1985).
16. **P.E. Parris and V.M. Kenkre**: Thermal runaway in ceramics arising from the temperature dependence of the thermal conductivity. *Phys. Status Solidi B* **200**, 39 (1997).
17. **E.B. Kulumbaev, V.E. Semenov, and K.I. Rybakov**: Stability of microwave heating of ceramic materials in a cylindrical cavity. *J. Phys. D: Appl. Phys.* **40**, 6809 (2007).
18. **M.S. Spotz, D.J. Skamser, and D.L. Johnson**: Thermal-stability of ceramic materials in microwave-heating. *J. Am. Ceram. Soc.* **78**, 1041 (1995).
19. **M. Alliouat, Y. Lecluse, J. Massieu, and L. Mazo**: Control algorithm for microwave sintering in a resonant system. *J. Microwave Power Electromagn. Energy* **25**, 25 (1990).
20. **G.O. Beale, F.J. Arteaga, and W.M. Black**: Design and evaluation of a controller for the process of microwave joining of ceramics. *IEEE Trans. Ind. Electron.* **39**, 301 (1992).
21. **V.E. Semenov and N.A. Zharova:** Thermal runaway and hot spots under controlled microwave heating. In *Advances in Microwave and Radio Frequency Processing*, M. Willert-Porada, ed. (Springer, Berlin, Germany, 2006); p. 482.
22. **Z.A. Munir, D.V. Quach, and M. Ohyanagi**: Electric current activation of sintering: A review of the pulsed electric current sintering process. *J. Am. Ceram. Soc.* **94**, 1 (2011).
23. **R. Raj, M. Cologna, and J.S.C. Francis**: Influence of externally imposed and internally generated electrical fields on grain growth, diffusional creep, sintering and related phenomena in ceramics. *J. Am. Ceram. Soc.* **94**, 1941 (2011).
24. **O. Guillon, J. Gonzales-Julian, B. Dargatz, T. Kessel, G. Schierning, J. Rathel, and M. Herrmann**: Field-assisted sintering technology/spark plasma sintering: Mechanisms, materials, and technology developments. *Adv. Eng. Mater.* **16**, 830 (2014).
25. **E.A. Olevsky and D.V. Dudina**: *Field-assisted Sintering: Science and Applications* (Springer International Publishing, Berlin/Heidelberg, Germany, 2018).
26. **M. Cologna, B. Rashkova, and R. Raj**: Flash sintering of nanograin zirconia in <5 s at 850 °C. *J. Am. Ceram. Soc.* **93**, 3556 (2010).
27. **C.E.J. Dancer**: Flash sintering of ceramic materials. *Mater. Res. Express* **3**, 102001 (2016).
28. **M. Yu, S. Grasso, R. Mckinnon, T. Saunders, and M.J. Reece**: Review of flash sintering: Materials, mechanisms and modelling. *Adv. Appl. Ceram.* **116**, 24 (2017).
29. **R.I. Todd, E. Zapata-Solvas, R.S. Bonilla, T. Sneddon, and P.R. Wilshaw**: Electrical characteristics of flash sintering: Thermal runaway of Joule heating. *J. Eur. Ceram. Soc.* **35**, 1865 (2015).
30. **K.I. Rybakov, Y.V. Bykov, A.G. Eremeev, S.V. Egorov, V.V. Kholoptsev, A.A. Sorokin, and V.E. Semenov:** Microwave ultra-rapid sintering of oxide ceramics. In *Processing and Properties of Advanced Ceramics and Composites VII*, M.M. Mahmoud, A.S. Bhalla, N.P. Bansal, J.P. Singh, R. Castro, N.J. Manjooran, G. Pickrell, S. Johnson, G. Brennecka, G. Singh, and D. Zhu, eds.; Ceramic Transactions, Vol. **252** (Wiley, Hoboken, New Jersey, 2015); p. 57.
31. **Y.V. Bykov, S.V. Egorov, A.G. Eremeev, V.V. Kholoptsev, K.I. Rybakov, and A.A. Sorokin**: Flash microwave sintering of transparent Yb:$(LaY)_2O_3$ ceramics. *J. Am. Ceram. Soc.* **98**, 3518 (2015).
32. **Y.V. Bykov, S.V. Egorov, A.G. Eremeev, V.V. Kholoptsev, I.V. Plotnikov, K.I. Rybakov, and A.A. Sorokin:** Sintering of oxide ceramics under rapid microwave heating. In *Processing, Properties and Design of Advanced Ceramics and Composites*, G. Singh, A. Bhalla, M.M. Mahmoud, R.H.R. Castro, N.P. Bansal, D. Zhu, J.P. Singh, and Y. Wu, eds.; Ceramic Transactions, Vol. **259** (Wiley, Hoboken, New Jersey, 2016); p. 233.
33. **Y.V. Bykov, S.V. Egorov, A.G. Eremeev, V.V. Kholoptsev, I.V. Plotnikov, K.I. Rybakov, and A.A. Sorokin**: On the mechanism of microwave flash sintering of ceramics. *Materials* **9**, 684 (2016).
34. **Y.V. Bykov, S.V. Egorov, A.G. Eremeev, I.V. Plotnikov, K.I. Rybakov, A.A. Sorokin, and V.V. Kholoptsev**: Effect of specific absorbed power on microwave sintering of 3YSZ ceramics. *IOP Conf. Ser.: Mater. Sci. Eng.* **218**, 012001 (2017).
35. **Y.V. Bykov, S.V. Egorov, A.G. Eremeev, I.V. Plotnikov, K.I. Rybakov, A.A. Sorokin, and V.V. Kholoptsev**: Flash sintering of oxide ceramics under microwave heating. *Tech. Phys.* **63**, 391 (2018).

https://doi.org/10.1557/jmr.2019.232 Published online by Cambridge University Press

© Materials Research Society 2019

36. **Y.V. Bykov, A.G. Eremeev, S.V. Egorov, V.V. Kholoptsev, I.V. Plotnikov, K.I. Rybakov, and A.A. Sorokin**: Ultra-rapid microwave sintering. *J. Phys.: Conf. Ser.* **1115**, 042005 (2018).
37. **Y.V. Bykov, S.V. Egorov, A.G. Eremeev, V.V. Kholoptsev, I.V. Plotnikov, K.I. Rybakov, A.A. Sorokin, S.S. Balabanov, and A.V. Belyaev**: Ultra-rapid microwave sintering of pure and Y_2O_3-doped $MgAl_2O_4$. *J. Am. Ceram. Soc.* **102**, 559 (2019).
38. **F. Trombin and R. Raj**: Developing processing maps for implementing flash sintering into manufacture of whiteware ceramics. *Am. Ceram. Soc. Bull.* **93**, 32 (2014).
39. **E. Sortino, J-M. Lebrun, A. Sansone, and R. Raj**: Continuous flash sintering. *J. Am. Ceram. Soc.* **101**, 1432 (2018).
40. **Y.V. Bykov, S.V. Egorov, A.G. Eremeev, V.V. Kholoptsev, I.V. Plotnikov, K.I. Rybakov, and A.A. Sorokin**: Additive manufacturing of ceramic products based on millimeter-wave heating. In *Abstract Book of the International Conference on High-Performance Ceramics (CICC-11)* (Kunming, China, 2019); p. 27.
41. **R. Raj**: Analysis of the power density at the onset of flash sintering. *J. Am. Ceram. Soc.* **99**, 3226 (2016).
42. **F. Kremer and J.R. Izatt**: Millimeter-wave absorption measurements in low-loss dielectric using an untuned cavity resonator. *Int. J. Infrared Millimeter Waves* **2**, 675 (1981).
43. **H.D. Kimrey and M.A. Janney:** Design principles for high-frequency microwave cavities. In *Microwave Processing of Materials*, W.H. Sutton, M.H. Brooks, and I.J. Chabinsky, eds.; Materials Research Society Symposium Proceedings, Vol. **124** (Materials Research Society, Pittsburgh, Pennsylvania, 1988); p. 367.
44. **Y.V. Bykov, A.G. Eremeev, M.Y. Glyavin, G.G. Denisov, G.I. Kalynova, E.A. Kopelovich, A.G. Luchinin, I.V. Plotnikov, M.D. Proyavin, M.M. Troitskiy, and V.V. Kholoptsev**: Millimeter-wave gyrotron research system. I. Description of the facility. *Radiophys. Quantum Electron.* **61**, 752 (2019).
45. **J.D. Jackson**: *Classical Electrodynamics* (Wiley, New York, New York, 1962).
46. **J. Narayan**: A new mechanism for field-assisted processing and flash sintering of materials. *Scr. Mater.* **69**, 107 (2013).
47. **R. Chaim**: Liquid film capillary mechanism for densification of ceramic powders during flash sintering. *Materials* **9**, 280 (2016).
48. **R. Chaim**: On the kinetics of liquid-assisted densification during flash sintering of ceramic nanoparticles. *Scr. Mater.* **158**, 88 (2019).
49. **S.V. Egorov, Y.V. Bykov, A.G. Eremeev, I.V. Plotnikov, K.I. Rybakov, A.A. Sorokin, and V.V. Kholoptsev**: Optical registration of shrinkage during ultra-rapid microwave sintering. In *Proceedings of the International Conference on "Synthesis and Consolidation of Powder Materials"* (Torus Press, Moscow, Russia, 2018); p. 277. doi: 10.30826/SCPM2018060 [in Russian].
50. **R. Roy, D. Agrawal, J. Cheng, and S. Gedevanishvili**: Full sintering of powdered-metal bodies in a microwave field. *Nature* **399**, 668 (1999).
51. **W.R. Tinga, W.A.G. Voss, and D.F. Blossey**: Generalized approach to multiphase dielectric mixture theory. *J. Appl. Phys.* **44**, 3897 (1973).
52. **D.A.G. Bruggeman**: Berechnung verschiedener physikalischer Konstanten von heterogenen Substanzen, I. Dielektriziätskonstanten und Leitfähigkeiten der Mischkörper aus isotropen Substanzen. *Ann. Phys.–Berlin, Series 5*, **24**, 636 (1935) [in German].
53. **K.I. Rybakov, V.E. Semenov, S.V. Egorov, A.G. Eremeev, I.V. Plotnikov, and Y.V. Bykov**: Microwave heating of conductive powder materials. *J. Appl. Phys.* **99**, 023506 (2006).
54. **K.I. Rybakov and V.E. Semenov**: Effective microwave dielectric properties of ensembles of spherical metal particles. *IEEE Trans. Microwave Theory Tech.* **65**, 1479 (2017).
55. **I.I. Volkovskaya, V.E. Semenov, and K.I. Rybakov**: Effective high-frequency permeability of compacted metal powders. *Radiophys. Quantum Electron.* **60**, 797 (2018).
56. **H. Sueyoshi, T. Hashiguchi, N. Nakatsuru, and S. Kakiuchi**: Effect of surface oxide film and atmosphere on microwave heating of compacted copper powder. *Mater. Chem. Phys.* **125**, 723 (2011).
57. **M.M. Mahmoud, G. Link, and M. Thumm**: The role of the native oxide shell on the microwave sintering of copper metal powder compacts. *J. Alloys Compd.* **627**, 231 (2015).
58. **K.I. Rybakov and M.N. Buyanova**: Microwave resonant sintering of powder metals. *Scr. Mater.* **149**, 108 (2018).
59. **C. Manière, G. Lee, T. Zahrah, and E.A. Olevsky**: Microwave flash sintering of metal powders: From experimental evidence to multiphysics simulation. *Acta Mater.* **147**, 24 (2018).
60. **G. Mie**: Beitrage zur optik trüber Medien, speziell kolloidaler Metallosungen. *Ann. Phys.* **330**, 377 (1908) [in German].
61. **H. Su and D.L. Johnson**: Master sintering curve: A practical approach to sintering. *J. Am. Ceram. Soc.* **79**, 3211 (1996).
62. **K.I. Rybakov and I.I. Volkovskaya**: Electromagnetic field effects in the microwave sintering of electrically conductive powders. *Ceram. Int.* **45**, 9567 (2019).
63. **Y. Bykov, A. Eremeev, M. Glyavin, V. Kholoptsev, A. Luchinin, I. Plotnikov, G. Denisov, A. Bogdashev, G. Kalynova, V. Semenov, and N. Zharova**: 24–84-GHz gyrotron systems for technological microwave applications. *IEEE Trans. Plasma Sci.* **32**, 67 (2004).
64. **L. Esposito, A. Piancastelli, Y. Bykov, S. Egorov, and A. Eremeev**: Microwave sintering of Yb:YAG transparent laser ceramics. *Opt. Mater.* **35**, 761 (2013).
65. **S.S. Balabanov, E.M. Gavrishchuk, A.M. Kut'in, and D.A. Permin**: Self-propagating high-temperature synthesis of Y_2O_3 powders from $Y(NO_3)_{3x}(CH_3COO)_{3(1-x)}{\cdot}nH_2O$. *Inorg. Mater.* **47**, 484 (2011).
66. **I.M. Robertson and G.B. Schaffer**: Some effects of particle size on the sintering of titanium and a master sintering curve model. *Metall. Mater. Trans. A* **40**, 1968 (2009).

https://doi.org/10.1557/jmr.2019.232 Published online by Cambridge University Press

© Materials Research Society 2019